BBA - Bioenergetics 1859 (2018) 8–18

Contents lists available at ScienceDirect

BBA - Bioenergetics

journal homepage: www.elsevier.com/locate/bbabio

Enzymatic and spectroscopic properties of a thermostable [NiFe]-hydrogenase performing H_2-driven NAD^+-reduction in the presence of O_2

Janina Preissler[a,1], Stefan Wahlefeld[a,1], Christian Lorent[a], Christian Teutloff[b], Marius Horch[a,*], Lars Lauterbach[a,*], Stephen P. Cramer[c], Ingo Zebger[a,*], Oliver Lenz[a,*]

[a] Technische Universität Berlin, Institut für Chemie, Sekr. PC14, Straße des 17. Juni 135, D-10623 Berlin, Germany
[b] Freie Universität Berlin, Fachbereich Physik, Arnimallee 14, D-14195 Berlin, Germany
[c] University of California, Department of Chemistry, One Shields Ave, Davis, CA 95616, USA

ARTICLE INFO

Keywords:
Hydrogenase
Hydrogen
Oxyhydrogen reaction
Nickel
Iron
Respiratory Complex I
Flavin
Iron-sulfur cluster
Pyridine nucleotide
Enzyme kinetics
Infrared vibrational spectroscopy
Electron paramagnetic resonance spectroscopy
Nuclear resonance vibrational spectroscopy
Biotechnology
Cofactor recycling

ABSTRACT

Biocatalysts that mediate the H_2-dependent reduction of NAD^+ to NADH are attractive from both a fundamental and applied perspective. Here we present the first biochemical and spectroscopic characterization of an NAD^+-reducing [NiFe]-hydrogenase that sustains catalytic activity at high temperatures and in the presence of O_2, which usually acts as an inhibitor. We isolated and sequenced the four structural genes, *hoxFUYH*, encoding the soluble NAD^+-reducing [NiFe]-hydrogenase (SH) from the thermophilic betaproteobacterium, *Hydrogenophilus thermoluteolus* TH-1^T (*Ht*). The *Ht*SH was recombinantly overproduced in a hydrogenase-free mutant of the well-studied, H_2-oxidizing betaproteobacterium *Ralstonia eutropha* H16 (*Re*). The enzyme was purified and characterized with various biochemical and spectroscopic techniques. Highest H_2-mediated NAD^+ reduction activity was observed at 80 °C and pH 6.5, and catalytic activity was found to be sustained at low O_2 concentrations. Infrared spectroscopic analyses revealed a spectral pattern for as-isolated *Ht*SH that is remarkably different from those of the closely related *Re*SH and other [NiFe]-hydrogenases. This indicates an unusual configuration of the oxidized catalytic center in *Ht*SH. Complementary electron paramagnetic resonance spectroscopic analyses revealed spectral signatures similar to related NAD^+-reducing [NiFe]-hydrogenases. This study lays the groundwork for structural and functional analyses of the *Ht*SH as well as application of this enzyme for H_2-driven cofactor recycling under oxic conditions at elevated temperatures.

1. Introduction

Enzymatic oxidation of dihydrogen (H_2) is a widespread trait in the microbial world and is used by many microbes to gain metabolic energy [1,2]. The reversible cleavage of H_2 into protons and electrons is mediated by complex metalloenzymes designated as hydrogenases [3]. In particular, the coupling of H_2 oxidation with aerobic respiration, i.e. the controlled Knallgas reaction ($H_2 + ½\ O_2 \rightarrow H_2O$), releases a high yield of free energy of $\Delta G^\circ = -237.2$ kJ per mol of H_2. Aerobic H_2 oxidation, however, requires hydrogenases that withstand the toxic effect of O_2. Among the different hydrogenase types, there is only one subclass that sustains H_2 oxidation in the presence O_2, namely the O_2-tolerant [NiFe]-hydrogenases [4]. One prominent member is the soluble NAD^+-reducing [NiFe]-hydrogenase (SH) from the betaproteobacterium *Ralstonia eutropha* H16 (*Re*), which is a well-known Knallgas bacterium possessing an H_2-driven chemolithoautotrophic metabolism [5]. *Re*SH directly couples H_2 oxidation with the reduction of NAD^+, thereby producing NADH, which is used both for energy conservation (through Complex I and the respiratory chain) and for CO_2 fixation via the Calvin cycle.

The *Re*SH is a bimodular enzyme consisting of four essential subunits, HoxFUYH, that harbor the [NiFe] active site, where H_2 conversion takes place, and the catalytic center for NAD^+ reduction, which carries a flavin mononucleotide (FMN) [6]. Electron transfer between the two active sites is mediated by four [4Fe4S] clusters and one [2Fe2S] site. Another FMN group has been suggested to be located close to the [NiFe] active site [7]. Two copies of the non-essential HoxI protein, whose function remains so far elusive, are also integral part of the *Re*SH [8]. The overall subunit composition as well as the cofactor arrangement of NAD^+-reducing [NiFe]-hydrogenases are reminiscent

* Corresponding authors.
E-mail addresses: marius.horch@gmx.de (M. Horch), lars.lauterbach@tu-berlin.de (L. Lauterbach), ingo.zebger@tu-berlin.de (I. Zebger), oliver.lenz@tu-berlin.de (O. Lenz).
[1] These authors contributed equally to the study.

http://dx.doi.org/10.1016/j.bbabio.2017.09.006
Received 24 May 2017; Received in revised form 17 August 2017; Accepted 28 September 2017
Available online 29 September 2017

of the situation in the peripheral arm of Complex I. In fact, it is anticipated that the SH represents a phylogenetic ancestor of Complex I [9,10], for which crystal structures are available [11]. Unfortunately, the *Re*SH has so far defied crystallization.

Three of four highly conserved cysteines coordinating the [NiFe] active site metal ions in the HoxH subunit are missing in the homologous subunit of Complex I (Nqo4 in case of *Thermus thermophilus*). According to amino acid sequence comparisons and numerous spectroscopic studies, the *Re*SH carries a [NiFe] center similar to that of canonical [NiFe]-hydrogenases [6,12,13]. Two of the four conserved cysteines serve as terminal nickel ligands, while the remaining two coordinate both the nickel and the iron ions. The iron is further equipped with one carbon monoxide and two cyanide ligands, which are supposed to maintain a low-spin Fe^{II} state throughout the catalytic cycle. The nickel ion, however, changes its redox state during H_2/H^+ turnover [6]. As the *Re*SH is catalytically active under aerobic conditions, a contact of the active site with O_2 is a very likely event. Nonetheless, the H_2 turnover rate remains at almost 100% even in the presence of 20% O_2, which makes *Re*SH the "world record holder" among O_2-tolerant, energy-converting [NiFe]-hydrogenases [14,15]. Moreover, the *Re*SH represents the first hydrogenase, for which a catalytic conversion of O_2 into water has been demonstrated [15]. The exceptional O_2 tolerance and the high turnover rates of the *Re*SH attracted scientists to employ the enzyme both in vitro and in vivo for H_2-driven NAD(P)H cofactor regeneration in biotechnologically relevant applications [16–19]. Though very efficient in NADH recycling, however, the *Re*SH has the disadvantage of being temperature-sensitive [20]. Both the lack of a crystal structure of an $NAD(P)^+$-reducing [NiFe]-hydrogenase and the limited temperature stability of *Re*SH have prompted us to seek out a thermostable version of this enzyme.

Hydrogenophilus thermoluteolus TH-1^T (*Ht*) has been described as an aerobic, facultatively chemolithoautotrophic, hydrogen-oxidizing microorganism, which – like *R. eutropha* – belongs to the phylogenetic class of betaproteobacteria [21]. It shows optimal chemolithoautotrophic growth with a H_2:O_2:CO_2 gas mixture of 7:2:1 at a temperature of 52 °C [22]. This suggests the presence of at least one O_2-tolerant [NiFe]-hydrogenase. Indeed, a recent study confirmed the presence of an SH-like enzyme in the moderate thermophile [23]. However, neither the corresponding genetic information nor a physiological or spectroscopic characterization of the *Ht*SH is so far available.

In this study, we present the DNA sequence of the structural genes of the four *Ht*SH subunits in addition to the gene encoding the *Ht*SH-specific endopeptidase. The *Ht*SH was recombinantly overproduced in *R. eutropha* and – upon purification – characterized by means of biochemical and spectroscopic methods. It turned out to be the first characterized [NiFe]-hydrogenase that performs H_2-driven NAD^+ reduction at elevated temperatures and in the presence of O_2.

2. Results and discussion

2.1. Identification of the genes encoding the NAD^+-reducing [NiFe]-hydrogenase of H. thermoluteolus

The draft sequence (published elsewhere) of the *H. thermoluteolus* TH-1^T genome revealed the *Ht*SH-related genes, *hoxF*, *hoxU*, *hoxY*, *hoxH*, and *hoxW*, which are apparently arranged as an operon (Fig. 1). Pairwise alignments of *Ht*SH and *Re*SH proteins (Fig. S1) revealed 40%, 37%, 44%, 46%, and 26% identical residues for HoxF, HoxU, HoxY, HoxH, and HoxW, respectively. Notably, the *H. thermoluteolus* TH-1^T genome does not contain a copy of the gene encoding the HoxI protein, which is a constituent of the *Re*SH [24].

2.2. Heterologous overproduction and purification of functional HtSH

For heterologous overproduction of the *Ht*SH in *R. eutropha* and subsequent purification, the *hoxFUYHW* genes were amplified by PCR and put under the control of the native SH promoter of *R. eutropha* as described in Materials and methods. Furthermore, a sequence encoding the *Strep*-tag II peptide was attached to the 5′ end of the *hoxF* gene. The resulting synthetic $hox_{strep}FUYHW$ operon was inserted into the broad-host range vector pEDY309 resulting in plasmid pJP09, encoding *Strep*-tagged *Ht*SH.

For enzyme purification, plasmid pJP09 was transferred into strain *R. eutropha* HF1054, in which the native *hoxFUYHWI* genes as well as *hoxG* encoding the large subunit of the membrane-bound [NiFe]-hydrogenases were eliminated by isogenic in-frame deletions. This prevented any "subunit mixing" between *Ht*SH and *Re*SH proteins. The transconjugant strain *R. eutropha* HF1054 (pJP09) was cultivated heterotrophically under oxygen-limited conditions as described previously [15,25]. In a first experiment, the H_2-driven NAD^+ reduction activity was measured in soluble extract of the recombinant cells. The activity was 2.50 ± 0.12 U mg^{-1} of protein (Table 1), suggesting the presence of functional *Ht*SH proteins. This result also demonstrates that the general [NiFe]-hydrogenase maturation machinery of *R. eutropha* [26–28] is able to synthesize and to deliver the active site constituents for the HoxH subunit of *Ht*SH.

The *Ht*SH protein was then purified to homogeneity by *Strep*-Tactin affinity and size exclusion chromatography as described in Materials and methods. From 10 g (wet weight) of cells, we routinely obtained 10–12 mg of protein with a specific H_2-driven NAD^+ reduction activity of 33.4 ± 0.6 U mg^{-1} of protein (measured at 50 °C, Table 1). The reverse reaction, namely NADH-driven H_2 production, was catalyzed with an activity of 1.0 ± 0.3 U mg^{-1} of protein. Using dithionite-reduced methyl viologen (MV) as artificial, low-potential electron donor, the H_2 production activity increased to 30 ± 5 U mg^{-1} of protein. SDS-PAGE performed with the *Ht*SH preparation revealed four protein bands assigned to the subunits HoxFUHY (Fig. 2).

2.3. Biochemical characterization of purified HtSH

Based on visual inspection of the protein bands after electrophoretic separation (Fig. 2), a ratio of approximately 1:1 of the two SH modules, HoxFU and HoxYH, was obtained only when Ni^{2+} (0.5 mM) and Mg^{2+} (5 mM) ions were present during the whole purification process. A similar observation has been made previously for the NAD^+-reducing [NiFe]-hydrogenase from *Rhodococcus opacus* [29]. Consequently, the following activity assays were conducted in the presence of Ni^{2+} and Mg^{2+} ions in addition to 2 μM FMN, the latter of which led to a shortened lag phase but did not change the maximal H_2 oxidation activity (Fig. S2). This suggests that FMN serves as an electron acceptor, and reduced FMN can reactivate those inactive *Ht*SH species which cannot be activated by H_2 alone. This mechanism is similar to the NADH-based reactivation of as-isolated *Re*SH [24,30]. Highest H_2-driven NAD^+ reduction activity for purified *Ht*SH (Fig. 3), however, was observed when the reductant TCEP (0.75 mM) was added in addition to FMN. Activity was maximal after a lag period of ca. 2.5 min. The removal of just TCEP led to a dramatic increase of the lag time (ca. 25 min), and the activity dropped to 25% of the value measured in the presence of TCEP (Fig. 3). The negative effect of the missing TCEP could be partly compensated through addition of catalytic amounts of NADH (5 μM), which led to the recovery of approx. 50% of the maximal activity and a halved lag phase (Fig. 3). This indicates that NADH supports reductive reactivation of aerobically purified *Ht*SH as previously observed for SH from *R. eutropha* [24,30]. A considerable further shortening of the lag phase was accomplished by increasing the protein concentration in the assay. In the presence of 0.8 μM *Ht*SH and only 2.5 μM NADH, it took only 4 min until full activity was developed (Fig. 3). This suggests that the rate of reductive reactivation can also be accelerated by intermolecular electron transfer between individual *Ht*SH enzymes. The likelihood of electron exchange between *Ht*SH enzymes is of course greater at higher protein concentration.

Based on the knowledge derived from the experiments described

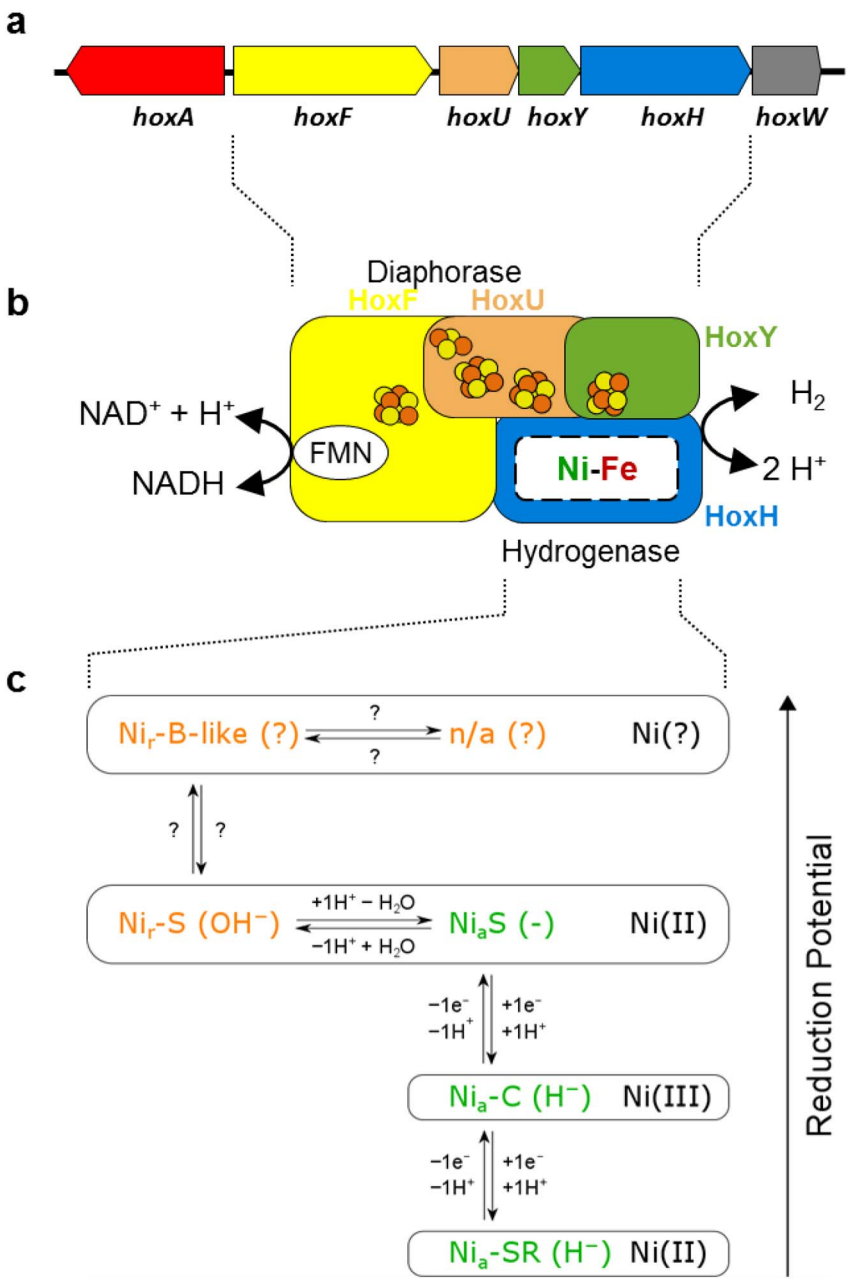

Fig. 1. Arrangement of the *Ht*SH-related genes (**a**), proposed subunit/cofactor composition (**b**), and observed active site redox states of *Ht*SH (**c**). Genes *hoxF*, *U*, *Y*, and *H* encode the subunits of the SH protein, while *hoxA* has presumably a regulatory function. Upon insertion of the [NiFe] active site, the *hoxW* gene product mediates cleavage of a C-terminal extension of the HoxH subunit. The proposed cofactor composition in **b** is derived from amino acid sequence comparisons with the corresponding subunits of *Re*SH and Complex I from *Thermus thermophilus* (see Fig. S1) and analogies to the well-characterized *Re*SH. The assignment of active site species and their interconversions shown in **c** is based on IR and EPR spectroscopic analyses (see below). Redox states highlighted in green belong to the catalytic conversion of H_2, while the orange ones represent inactive states that – except for Ni_r-S – require reductive treatment to be converted into the Ni_a-S state. The unassigned oxidized state labelled with n/a is unprecedented (see below).

Table 1
Purification of *Ht*SH protein enzyme by affinity chromatography.

Fraction[a]	Volume (mL)	Protein concentration (mg/mL)	Total protein (mg)	Specific activity (U mg^{-1})[b]	Total activity (U)	Yield (%)	Enrichment factor
SE	40	29.2	1168	2.5 ± 0.1	2920	100	1
AC	1.4	29.7	41.6	12.1 ± 0.1	502	17	4.8
SEC	2.4	4.9	11.7	33.4 ± 0.6	391	13	13.4

[a] The *Ht*SH protein was purified from soluble cell extracts (SE) by *Strep*-Tactin affinity chromatography (AC) and subsequent size exclusion chromatography (SEC) as described in Materials and methods.

[b] Activity was determined by H_2-dependent NAD^+ reduction in 50 mM bis-Tris, pH 6.5, supplemented with 1 mM NAD^+, 0.5 mM $NiCl_2$, 5 mM $MgSO_4$, 2 μM FMN, and 0.75 mM TCEP at a temperature of 50 °C. One Unit (U) corresponds to the amount of converted substrate (in μmol) in 1 min. Values of a representative purification are shown.

above, $NiCl_2$, $MgSO_4$, FMN, and TCEP were added to the following activity assays, unless stated otherwise. Using this standard protocol at a fixed temperature of 50 °C, we first determined the H_2-dependent NAD^+ reduction activity of purified *Ht*SH at different pH values. This was accomplished with a universal buffer that spanned the entire pH range from pH 4.5–9 (Fig. 4) as well as with three buffers with different pH ranges (Fig. S3). From both experiments, an optimum pH of 6.5 was derived. This is in marked contrast to *Re*SH that performs best at pH 8.0 [20,30] (Table 2), where the *H. thermoluteolus* enzyme showed only about 10% of the maximal H_2-driven NAD^+ reduction activity of 50 ± 4 U mg^{-1} of protein (measured at pH 6.5, Fig. 4).

In order to elucidate the origin of the unusual pH optimum, the

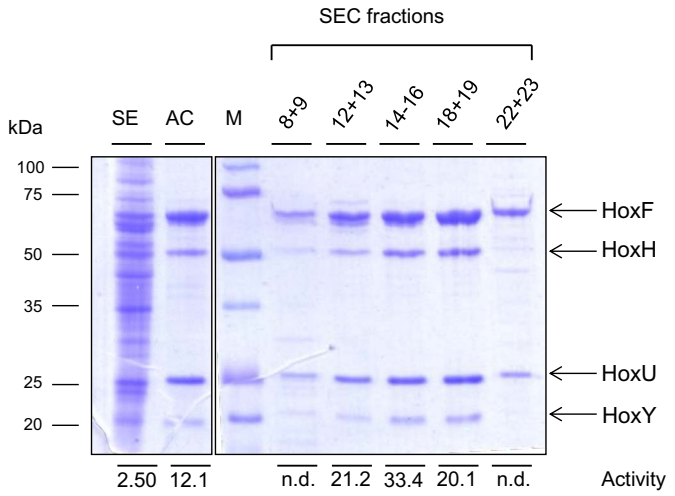

Fig. 2. Purification of the *Ht*SH protein. A protein amount of 30 µg of soluble extract (SE) and 5 µg of *Ht*SH purified by affinity chromatography (AC) and selected fractions (from the subsequent size exclusion chromatography (SEC) were electrophoretically separated on a 12% SDS-polyacrylamide gel and subsequently stained with Coomassie brilliant blue. The specific H_2-driven NAD^+ reduction activity (U mg^{-1} of protein) of each fraction is specified below. Lane M contains marker proteins and their corresponding molecular weights are given on the left hand side.

enzymatic reactions of the two SH modules were tested separately in a pH-dependent manner (Fig. 4). First, the HoxFU-catalyzed NADH:-benzyl viologen oxidoreductase activity was measured as described in Materials and methods. Maximum activity of 64 ± 5 U mg^{-1} of protein was reached at approximately pH 10, which is qualitatively consistent with the observations made previously for the HoxFU module of the *Re*SH [31]. The H_2:benzyl viologen oxidoreductase activity of the HoxHY module, however, was found to be optimal at approximately pH 7.0. These results indicate that the pH optimum of the *Ht*SH is primarily dictated by the intrinsic bias of the H_2/H^+-cycling module of the holoenzyme.

Measurements of the H_2-dependent NAD^+ reduction activity of purified *Ht*SH at different temperatures were performed in bis-Tris buffer at pH 6.5 and revealed a maximal activity of 71.0 ± 0.3 U mg^{-1} of protein at a temperature of 80 °C (Fig. 5). This is in sharp contrast to *Re*SH, which quickly loses activity at temperatures higher than 35 °C [20] (Table 2). At 33 °C, which is the temperature optimum of *Re*SH activity [30], *Ht*SH showed less than 20% of the maximal activity.

In a next series of experiments, we determined the Michaelis-Menten constants (K_M) for the natural substrates of the *Ht*SH. The K_M value for NAD^+ was evaluated based on the H_2-driven NAD^+ reduction activity of the enzyme and revealed to lie at 469 µM (Fig. S4) which is close to 560 µM, the value determined for *Re*SH [30]. Activity measurements of the *Ht*SH-mediated benzyl viologen reduction activity in the presence of various NADH concentrations resulted in a K_M^{NADH} of 1.2 mM (Fig. S5), which is surprisingly high when compared to the corresponding value of 80 µM determined for the *Re*SH [30]. This suggests that the main physiological role of *Ht*SH enzyme is H_2-driven NAD^+ reduction.

A value of 42 ± 3 µM was determined for the apparent Michaelis-Menten constant, $K_{M,}^{app}$ for H_2 during H_2-driven NAD^+ reduction of the enzyme (Fig. S6), which is comparable to that measured for *Re*SH (37 µM, [30], Table 2).

2.4. Cofactor content and O_2 tolerance of HtSH

Fluorescence determination revealed 1.07 FMN per SH tetramer. Using inductively coupled plasma optical emission spectrometry, 14.2 ± 0.2 Fe and 2.4 ± 0.1 Ni per SH molecule were detected. On the basis of conserved amino acid residues that are involved in Fe-S cluster coordination in Complex I, 19 iron atoms are expected in addition to one nickel in the catalytic center of the hydrogenase module (Fig. 1, Fig. S1). Additional information on the type of iron-sulfur clusters present in *Ht*SH was obtained by nuclear resonance vibrational spectroscopy (NRVS). NRVS is a synchrotron-based vibrational spectroscopic technique that selectively probes iron-specific normal modes and has been shown to provide details on [NiFe]-hydrogenase cofactor structure and composition [42,43]. The partial vibrational density of states (PVDOS) for oxidized *Ht*SH is presented in Fig. S7. The band at 414 cm^{-1} is characteristic for the presence of a [2Fe2S] cluster [44], which is supposed to be coordinated by the HoxU subunit. Of the 19 irons in *Ht*SH, 16 are expected to be constituents of [4Fe4S] clusters. Indeed, also the spectral pattern between 0 and 400 cm^{-1} is very similar to that of *Re*SH [43] and a [4Fe4S] cluster-containing ferredoxin [45] (Fig. S7), which indicates dominant contributions of [4Fe4S] cluster species. Thus, these results support the presence of four [4Fe4S] clusters and one [2Fe2S] species in *Ht*SH.

Consistent with the chemolithoautotrophic growth capacity of the host organism under aerobic conditions, the isolated *Ht*SH showed sustained H_2-driven NAD^+ reduction activity in the presence of O_2

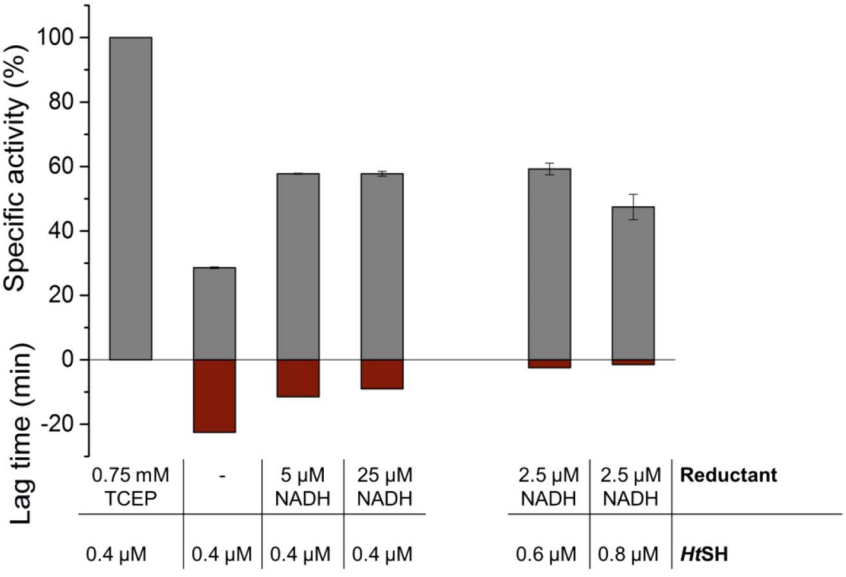

Fig. 3. Dependence of H_2-driven NAD^+ reduction activity of purified *Ht*SH protein on the addition of reductants TCEP and NADH. The assay was performed at 50 °C in 50 mM bis-Tris, pH 6.5, supplemented with 1 mM NAD^+, 0.5 mM $NiCl_2$, 5 mM $MgSO_4$, 2 µM FMN, and varying amounts of TCEP, NADH and *Ht*SH. The lag time refers to the time elapsed from assay start until full activity was achieved. 100% activity refers to 19 U mg^{-1} of protein.

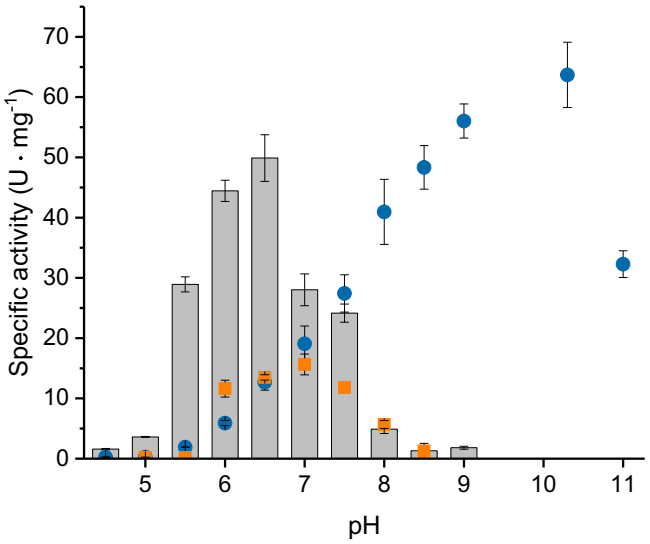

Fig. 4. Activity of purified *Ht*SH protein at different pH values. The graph depicts the H_2-dependent NAD^+ reduction activities of *Ht*SH (grey bars) as well as the H_2:benzyl viologen (orange symbols) and NADH:benzyl viologen (blue symbols) oxidoreductase activities of the individual *Ht*SH modules. The measurements were performed as described in Materials and methods with 45 nM of *Ht*SH in an universal buffer composed of 16 mM citrate, 16 mM Tris, and 16 mM glycine. Activities were measured at a temperature of 50 °C in the presence of either of 1 mM NAD^+, 1 mM NADH, or 5 mM benzyl viologen, in addition to 0.5 mM $NiCl_2$, 5 mM $MgSO_4$, 2 μM FMN, and 0.75 mM TCEP.

(Table 3). However, its O_2 tolerance revealed to be lower than that of the *Re*SH (Table 3, Table 2). While the *Re*SH preserves approximately 100% activity observed at 20% O_2 (measured at 30 °C in Tris/HCl buffer, pH 8) [14,15], the *H. thermoluteolus* enzyme showed at 10% O_2 less than 20% of the activity measured in the absence of O_2. At 2% O_2, it displayed only 50% of the activity observed under anaerobic conditions. However, at low O_2 pressure (0.2%), *Ht*SH activity remained at almost 100% (Table 3). In this respect, it is noteworthy that the intracellular O_2 concentration in living cells is generally much lower than the external one. This explains why *H. thermoluteolus* cells grow well with H_2 and CO_2 even at ambient O_2 concentrations, although the isolated enzyme is more O_2 sensitive than the SH from *R. eutropha*.

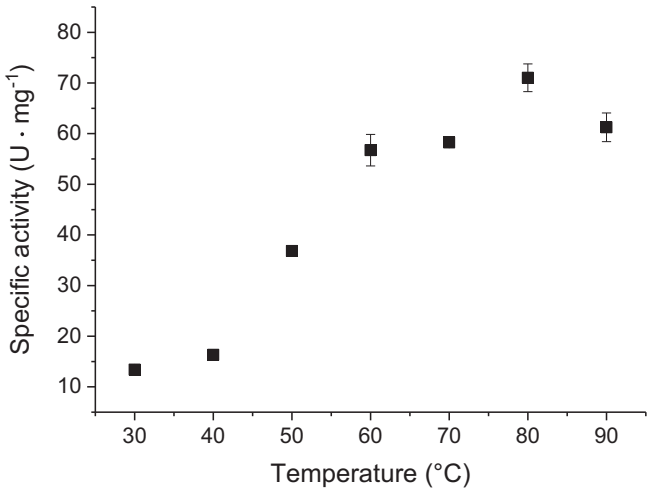

Fig. 5. Temperature dependence of the H_2-dependent NAD^+ reduction activity of purified *Ht*SH protein. The measurements were performed as described in Materials and methods with 45 nM of *Ht*SH in 50 mM bis-Tris buffer, pH 6.5, containing 1 mM NAD^+, 0.5 mM $NiCl_2$, 5 mM $MgSO_4$, 2 μM FMN, and 0.75 mM TCEP. If the error bars are not visible, they are equal or smaller than the symbol size.

Table 3
H_2-driven NAD^+ reduction activity of the *Ht*SH protein[a] in the presence of various O_2 concentrations.

$O_2/H_2/N_2$ fractions[b] (% v/v)	$[O_2]$ (μM)	Hydrogenase activity in the presence of O_2 (U mg^{-1} of protein)[c]	k_{cat} (s^{-1})	Hydrogenase activity (%)
0/33.33/66.66	0.00	16 ± 2	45.9	100
0.2/33.33/66.46	1,9	15 ± 4	43.0	94.2
2/33.33/64.66	18,8	7.7 ± 0.3	21.5	49.8
10/33.33/56.66	94,0	1.3 ± 0.5	3.6	16.6

[a] *Ht*SH was purified by affinity chromatography as described in Materials and methods.
[b] For each O_2 concentration, a fixed volume of H_2-saturated buffer was mixed with various proportions of O_2- and N_2-saturated buffers. The gas phase contained the corresponding gas mixtures.
[c] H_2-mediated NAD^+ reduction activity was measured at 50 °C and pH 6.5.

Table 2
Comparison of soluble, $NAD(P)^+$-reducing [NiFe] hydrogenases.[a]

Organism	*H. thermoluteolus* TH-1[T]	*R. eutropha* H16	*Synechocystis* sp. PCC 6803	*Pyrococcus furiosus*
Designation	SH	SH	Bidirectional hydrogenase	SH1
Subunit composition	HoxHYFU	$HoxHYFUI_2$ [24]	HoxHYFUE [32]	αδβγ [33]
Molecular weight (kDa)	168	207 [24]	180 [32]	153 [33]
K_M H_2 (μM)	42	37 [30]	11.3 [34][b]	140 [33]
Physiological electron acceptors/donors	NAD^+	NAD^+	$NAD(P)^+$/NAD(P)H, $ferredoxin_{red}$, $flavodoxin_{red}$ [35,36]	$NAD(P)^+$
K_M $NAD(P)^+$ (μM)	469 (NAD^+)	560 (NAD^+) [30]	n.p.	40 ($NADP^+$) [33]
k_{cat} for H_2-driven $NAD(P)^+$ reduction (s^{-1})	150 s^{-1}	485 s^{-1} [8]	n.p.	99 s^{-1} (NAD^+) [33] 38–89 s^{-1} ($NADP^+$) [37]
v_{max} for NAD(P)H-driven H_2 production	0.9 U mg^{-1}	1.2 U mg^{-1}	2.81 (U mg^{-1}) [32]	1.5–2 U mg^{-1} (NADPH)
T_{opt}	80 °C	35 °C [20]	60 °C [32]	80 °C [38,39]
pH_{opt}	6.5	8 [20,30]	6.3 [32]	8.4 [38]
Behavior towards O_2	Moderately O_2-tolerant ~50% H_2-dependent NAD^+ reduction activity[c] in the presence of 19 μM O_2	O_2-tolerant, ~85% H_2-dependent NAD^+ reduction activity[c] in the presence of 470 μM O_2 [15]	O_2-sensitive, no catalytic activity in the presence of O_2; can be rapidly reactivated under reducing conditions [40]	Moderately O_2-tolerant, ~25% of H_2 oxidation activity[d] in the presence of 14 μM O_2 [41]

n.p.; not published.
[a] Note that values are only limitedly comparable since the assay conditions were not identical.
[b] Value has been determined for the bidirectional hydrogenase from the *Synechocystis* sp. relative, *Anabaena variabilis*.
[c] Compared to the activity measured in the absence of O_2. Activities were measured spectrophotometrically in solution.
[d] Compared to the activity measured in the absence of O_2. Activities were measured electrochemically with immobilized enzyme at oxidizing potential.

Table 4
CO and CN stretching frequencies (cm^{-1}) of IR-spectroscopically observed *Ht*SH [NiFe] active site species.

Assignment	ν(CO)	ν(CN)	
n/a[a]	1993	2081	2090
Ni_r-B-like	1964	2087	2098
Ni_r-S	1936	2058	2071
Ni_a-S	1951	2076	2089
Ni_a-C	1971	2076	2089
Ni_a-SR	1958	2062	2076
Ni_a-SR′	1943	2048	2062
Ni_a-SR″	1934	2048	2062

[a] Not assigned. Oxidized active site species of unknown structure.

2.5. Spectroscopic characterization of HtSH

To gain insight into structure and function of the metal cofactors, in particular of the [NiFe] active site, *Ht*SH samples treated with different redox agents were characterized by IR and EPR spectroscopy. For both types of spectroscopic measurements, samples were prepared under identical conditions to guarantee comparability of the results. In addition, IR spectro-electrochemical experiments were performed to provide insight into equilibria between the individual redox states of the [NiFe] active site. All IR data are displayed as second derivative spectra where the maximum of an absorption band appears as a sharp negative peak. Peak positions derived from IR and EPR spectroscopy as well as their assignment to individual cofactors and redox states are summarized in Tables 4 and 5, respectively.

IR spectra of as-isolated *Ht*SH exhibit up to three distinct bands at 1993, 1964, and 1936 cm^{-1} (Fig. 6, trace a). Signals in this spectral region are generally associated with the stretching vibration of the intrinsic CO ligand of the [NiFe] active site, and different vibrational frequencies reflect distinct redox/structural states of this cofactor [3,46–49]. The three individual CO stretching vibrations of oxidized *Ht*SH are separated by approximately 30 cm^{-1}, which is exceptional for active site species of oxidized [NiFe] hydrogenases. This observation suggests that the active site of as-isolated *Ht*SH can adopt three configurations that strongly differ in terms of structural and/or electronic properties. The signal at 1964 cm^{-1} may reflect the apparently EPR-silent "Ni_r-B-like" state (Fig. 1), which was previously detected for *Re*SH and other NAD(P)$^+$-reducing [NiFe] hydrogenases [6,8,12,40,50,51], and the band at 1936 cm^{-1} is assigned to the Ni_r-S state (see below). The signal at 1993 cm^{-1}, however, is unprecedented and absent in as-isolated *Re*SH [8,50,52–54]. According to relative intensities of the CO stretching bands, the contributions of the three different states varied across different as-isolated *Ht*SH preparations. The unusual signal at 1993 cm^{-1}, however, generally represented the dominant species. To the best of our knowledge, such a high CO stretching frequency has not been observed for any [NiFe] hydrogenase to date. This suggests unusually high oxidation states of the metal ions, e.g. formation of ferric iron [55], or unusual structural features at or in close vicinity of the [NiFe] active site. In general, such observations and the appearance of multiple oxidized states may result from the contact with O_2 during and after protein isolation [50,56]. Importantly, all IR-spectroscopically detected oxidized species of the *Ht*SH active site can be activated under reducing conditions (Fig. 6, traces b and c), as observed previously for, e.g., *Re*SH [50]. This indicates that the modifications reflected by the unusual signal at 1993 cm^{-1} are reversible and not related to oxidative damage.

Table 5
g-Values of *Ht*SH cofactor species observed by EPR spectroscopy.

Assignment	g_1	g_2	g_3
[3Fe4S]	2.004	1.982	
[2Fe2S]	2.026	1.935	
[NiFe]: Ni_a-C	2.210	2.139	2.013
[NiFe]: n/a[a]	2.260	2.127	2.034
FMN	2.003		

[a] Not assigned.

The EPR spectrum of as-isolated *Ht*SH was measured at 10 K (Fig. 6, trace d) and exhibits a minor signal, presumably related to a [3Fe4S] cluster. Since no such cofactor is expected for native *Ht*SH, this feature likely reflects the (partial) oxidative damage of one or more [4Fe4S] clusters, which is in line with preparation-dependent variations of the signal intensity. This situation is reminiscent of *Re*SH and the related NAD$^+$-reducing hydrogenase from *Rhodococcus opacus* (*Ro*), both of which exhibit similar signals related to (non-native) [3Fe4S] species [8,13,53,57–60]. Furthermore, a weak rhombic signal, detected at 35 K, (Fig. S8, trace a) is presumably related to a paramagnetic [NiFe] active site state of as-isolated *Ht*SH. Signals related to typical active site species of oxidized "standard" [NiFe] hydrogenases, however, were not detected, which is consistent with previous findings for NAD(P)$^+$-reducing hydrogenases from other organisms [6,8,12,13,40,53,57–61].

Upon addition of the mild reducing agents TCEP and NADH to as-isolated *Ht*SH, bands at 1993 and 1964 cm^{-1} disappeared from the IR spectrum in favor of two new absorption features at 1971 and 1951 cm^{-1} (Fig. 6, trace b). The former is ascribed to the Ni_a-C state of the enzyme, which is in line with previous studies showing that Ni_a-C exhibits the highest CO stretching frequency among all catalytically active [NiFe] species [3]. The second band, observed at 1951 cm^{-1}, is assigned to the one-electron more oxidized Ni_a-S state, consistent with an intensity decrease upon hydrogen incubation of the enzyme (see below and Fig. 6, trace c). In *Re*SH and soluble hydrogenase I (SH1) from the hyperthermophilic organism *Pyrococcus furiosus* (*Pf*), this state corresponds to signals at 1946 cm^{-1} [50] and 1950 cm^{-1} [51], respectively (note that *Pf*SH1 differs from *Ht*SH and *Re*SH in terms of its subunit and cofactor composition [6]). The band at 1936 cm^{-1} gains intensity upon incubation of as-isolated *Ht*SH with TCEP and NADH (Fig. 6, traces a and b) indicating that it reflects a partially reduced [NiFe] species with a formal Ni^{II} oxidation state. Since this CO stretching frequency is clearly lower than those observed for most other *Ht*SH [NiFe] active site species, we tentatively assign this intermediate to the deprotonated Ni_r-S subspecies, which features a bridging OH^- ligand.

The corresponding EPR spectrum of TCEP/NADH-reduced *Ht*SH was recorded at 35 K and clearly shows the hydride-containing Ni_a-C state (Ni^{III}, $S = 1/2$), consistent with the corresponding assignment of the strong IR absorbance at 1971 cm^{-1}. Moreover, signals attributed to a [2Fe2S] cluster (consistent with the results obtained by NRVS, Fig. S7) and a flavin radical species were detected (Fig. 6, trace e). These assignments are supported by simulation and subsequent summation of the individual components (Fig. 6, trace e, dashed line) and consonant with previous assignments for *Re*SH and *Ro*SH [8,12,13,40,53,57–60,62]. Measurements performed at 10 K (Fig. S8, trace b) revealed an additional broad signal at $g = 1.85$, possibly reflecting a [4Fe4S] cluster.

Upon incubation of *Ht*SH with H_2 (in the presence of TCEP and NADH), the 1971 cm^{-1} band, assigned to the Ni_a-C state, becomes the most intense signal of the IR spectrum, and corresponding CN stretching vibrations of this catalytic intermediate can be identified at 2076 and 2089 cm^{-1} (Fig. 6, trace c). Moreover, a new redox species is formed as indicated by the appearance of an absorption band at 1958 cm^{-1} (Fig. 6, trace c). According to spectro-electrochemical measurements (Fig. S9, traces b and c), an enrichment of this species requires lower potentials than that of the Ni_a-C state. Therefore, we attribute this signal to the fully reduced Ni_a-SR species with corresponding CN stretching bands at 2076 and 2062 cm^{-1}, which is in line with band assignments for *Pf*SH1 [51]. In case of *Re*SH, a similar set of signals, including an identical CO stretching band at 1958 cm^{-1}, has been assigned to the Ni_a-SR2 state [6,12,50]. In the current case,

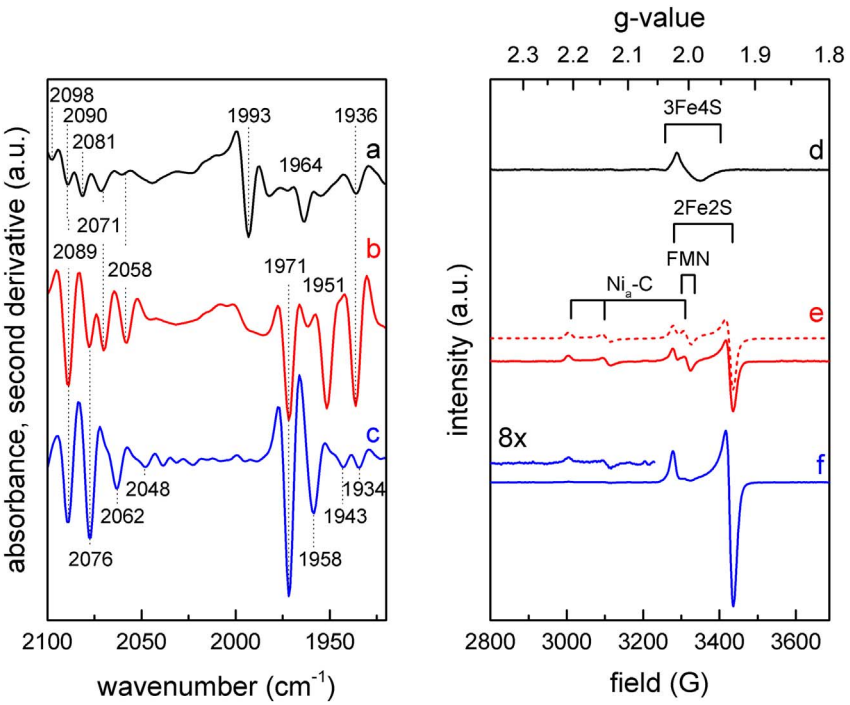

Fig. 6. IR (left) and EPR (right) spectra of *Ht*SH recorded under different redox conditions. Samples were prepared as described in "Materials and methods" and measured in the as-isolated, oxidized state (black spectra) or in their reduced states (red spectra: samples reduced with TCEP and NADH; blue spectra: samples reduced with TCEP, NADH, and H_2). IR spectra were acquired at 10 °C, while EPR spectra were recorded at either 10 K (d) or 35 K (e, f).

however, this assignment is less plausible since CO stretching bands of *Ht*SH active site redox states appear to be generally higher in frequency than their counterparts in *Re*SH. Two further weak bands at 1943 and 1934 cm^{-1} (Fig. 6, trace c) might reflect Ni_a-SR′ and Ni_a-SR″ subspecies of the reduced state [12,50]. Consistently, these states were observed as bands at 1940 (Ni_a-SR′) and 1931 cm^{-1} (Ni_a-SR″) for *Pf*SH1, which also exhibits generally higher CO stretching frequencies than *Re*SH [51]. Observation of these two subspecies provides further support for the assignment of the 1958 cm^{-1} band to Ni_a-SR as there is no other signal in the IR spectrum of *Ht*SH that could be attributed to the main component of this species.

The EPR spectrum of H_2-incubated *Ht*SH, recorded at 35 K, is dominated by the signal of the [2Fe2S] cluster (Fig. 6, trace f) confirming further enzyme reduction. In contrast to the IR data, this EPR spectrum exhibits only trace amounts of the Ni_a-C state. However, in addition to broad features at positions typical for reduced [4Fe4S] cofactors ($g = 1.83$), an EPR spectrum recorded at 6.5 K (see Fig. S8, trace c) reveals pronounced broadened signals in the field range characteristic for the Ni_a-C state, indicating strong magnetic coupling of the active site with another paramagnetic species. This temperature dependence of the Ni_a-C signal pattern can be explained by fast spin-lattice relaxation of an Fe-S cluster near the [NiFe] site, leading to enhanced relaxation and broadening of the Ni_a-C signal until its disappearance at higher temperatures. Similar magnetic interactions have been described in detail for "standard" [NiFe] hydrogenases [63,64], and particularly pronounced coupling effects were also reported for *Pf*SH1 [39], *Pyrococcus furiosus* ferredoxin [65], and individual clusters of homologous respiratory Complex I [66–68]. For the Ni_a-C state of *Ht*SH, this effect appears to be most pronounced for the NADH/TCEP/H_2-treated sample. Assuming that unspecific, preparation-dependent effects can be excluded, this observation suggests that spin-lattice relaxation is accelerated by coupling to a paramagnetic cofactor ([4Fe4S] species) that is barely reduced by TCEP/NADH alone.

To support band assignments and gain insight into the reversibility of redox reactions at the [NiFe] active site of *Ht*SH, initial IR spectroelectrochemical measurements and gas-exchange experiments were performed (Fig. S9, Fig. S10). As summarized in Table 4, these studies allowed a preliminary assignment of the CN stretching bands for all detected [NiFe] active site states. The monitored interconversions also confirmed the above-made assignments of the individual [NiFe] active site species, and the corresponding redox equilibria could be established (Fig. 1c). Remarkably, after reduction of as-isolated *Ht*SH and subsequent re-oxidation, the [NiFe] active site species reflected by the unusual 1993 cm^{-1} band did not re-appear (Fig. S9, Fig. S10). Thus, we propose that the reaction resulting in this particular species is kinetically hindered, suggesting a pronounced structural reorganization. In line with the unusually high CO stretching frequency, this observation supports the idea that this oxidized state differs considerably from other typical [NiFe] active site intermediates.

3. Conclusion

Here, we provide the first combined biochemical and spectroscopic characterization of a NAD^+-reducing [NiFe]-hydrogenase that is both thermostable and O_2-tolerant. The enzyme originates from the thermophile *Hydrogenophilus thermoluteolus* TH-1^T [21], and its corresponding structural genes were heterologously overexpressed in the mesophilic host *Ralstonia eutropha* H16. This procedure resulted in the formation of catalytically active *Ht*SH protein, which clearly shows that the hydrogenase-specific maturation machinery from *R. eutropha* [5] is capable of synthesizing and inserting the $NiFe(CN)_2CO$ cofactor into the large hydrogenase subunit of *Ht*SH. Taking into account the successful heterologous overproduction of SH from *Rhodococcus opacus* [69], *R. eutropha* seems to be an excellent host for synthesis and isolation of catalytically active SH proteins from bacterial species that are so far unamenable to genetic engineering.

Table 2 shows biochemical and structural properties of the *Ht*SH in comparison with those of other soluble $NAD(P)^+$-reducing [NiFe]-hydrogenases. The isolated *Ht*SH is a heterotetrameric enzyme with a turnover frequency of ca. 150 s^{-1} for H_2-driven reduction of NAD^+ at pH 6.5 and 50 °C. In terms of biotechnologically relevant cofactor regeneration [19], the *Ht*SH is complementary to *Pf*SH1, which preferably reduces $NADP^+$ in a H_2-dependent manner at high temperature [33]. Although to a lesser extent when compared to *Re*SH, *Ht*SH shows catalytic H_2-mediated NAD^+ reduction in the presence of O_2 in solution assays. For *Pf*SH1, O_2-tolerant H_2 oxidation (but not $NAD(P)^+$ reduction) has so far only be shown electrochemically with immobilized enzyme [41]. Though phylogenetically closely related to *Ht*SH and

*Re*SH, the purified bidirectional [NiFe]-hydrogenase from *Synechocystis* sp. seems to be rather unstable and is rapidly inactivated by O_2. The well-characterized and extraordinary O_2-tolerant *Re*SH, in contrast, shows good stability and highest activity at moderate temperatures and pH 8, but quickly loses activity at temperatures above 35 °C [20]. In summary, the *Ht*SH represents an attractive candidate for biotechnological applications, e.g., as an NADH regeneration catalyst in enzymatic cascades that rely on high temperatures and O_2 as a co-substrate.

EPR, IR and NRV spectroscopic analyses of the *Ht*SH protein revealed the occurrence of FMN, [2Fe2S], and [4Fe4S] cluster species as well as typical active site states that have been observed for other soluble NAD(P)$^+$-reducing [NiFe] hydrogenases [6,40,51]. These include the Ni_r-B-like state that is not directly involved in H_2/H^+ cycling as well as the Ni_a-S, Ni_a-C, and Ni_a-SR states which are generally accepted to be intermediates of the catalytic cycle. While the Ni_a-C state was identified both by IR and EPR spectroscopy, all other states are EPR-silent and were assigned based on IR spectroscopic analyses only. Interestingly, the Ni_a-C signal in the EPR spectrum of H_2-treated *Ht*SH was mainly observed at temperatures below 10 K, presumably due to fast spin-lattice relaxation related to magnetic coupling with another cofactor that is paramagnetic under these reducing conditions. This observation represents an important finding that could explain why Ni_a-C and other paramagnetic active site species have often not been observed for NAD(P)$^+$-reducing [NiFe] hydrogenases [6,40]. Furthermore, the as-isolated, oxidized *Ht*SH exhibits a CO stretching vibration at 1993 cm^{-1}, which is extremely high in frequency and so far unprecedented for [NiFe]-hydrogenases. This unusual vibrational band most likely reflects an alternative geometry and/or coordination environment of the hetero bimetallic active site. Since no crystallographic data is available yet, further spectroscopic investigations are currently in progress to gain detailed insight into the structure this novel species.

4. Materials and methods

4.1. Construction of the synthetic P_{SH}-hox_{strep}FUYHW operon, growth conditions, and protein purification

The *Ht*SH-derived gene cluster containing *hoxFUYHW* was amplified by PCR using the primers

5′-agaacctgtacttccagggcgcaacacgaggaggaggaac-3′

and

5′-ctcggtacccggggatccatacctcctcttcgtgggtgaaaaaac-3′,

and genomic DNA from *Hydrogenophilus thermoluteolus* TH-1^T as the template. The underlined bases of the primers are complementary to plasmid pGE837, which is a pCM66 [70] derivative carrying a *Xba*I-*Bam*HI-cut fragment from plasmid pGE770 [15] with $P_{SH\text{-}Strep}$*hoxF* from *Ralstonia eutropha* H16 followed by a sequence encoding a GG-GENLYFQG linker with a TEV cleavage site (underlined residues). Plasmid pGE837 was linearized by inverted PCR using primers 5′-atggatccccgggtaccga-3′ and 5′-gccctggaagtacaggttctcg-3′, and the 7.9-kb product served as recipient of the *Ht hoxFUYHW* PCR amplicon, which was inserted according to the Gibson Assembly® manual (New England BioLabs). The resulting plasmid carries the *Ht hoxFUYHW* genes under control of the SH promoter of *R. eutropha* [71], whereby the 5′ end of the *hoxF* gene was equipped with a linker sequence and a *Strep*-tag II-encoding sequence. A P_{SH}-hox_{Strep}*FUHYW* fragment was cut out with *Eco*53KI and XbaI, and the resulting 5.7 kb fragment was inserted into the *Sca*I-XbaI-cut vector pEDY309 [72]. This yielded plasmid pJP09, which was subsequently transferred by conjugation to *R. eutropha* HF1054, which is a HF424 [73] derivative carrying an additional in-frame deletion in the *hoxI* gene.

Strain *R. eutropha* HF1054 (pJP09) was grown heterotrophically in a mineral salts medium containing a mixture of 0.05% (w/v) fructose and 0.4% (v/v) glycerol (FGN medium) at 30 °C as described previously [25]. Upon reaching an optical density at 436 nm of 9–11, the culture was collected, and the cells were harvested by centrifugation at 8850 × *g* for 15 min at 4 °C. The cell pellet was resuspended in 50 mM KPO_4, pH 7.2, containing 15–20% (v/v) glycerol, 5 mM $MgCl_2$, 0.5 mM $NiCl_2$, and protease-inhibitor cocktail (EDTA-free Protease Inhibitor, Roche). The extract was furthermore supplemented with 5 mM NAD$^+$ in order to keep the *Ht*SH in the oxidized state, which is thought to prevent extensive oxidative damage through reactive oxygen species [15]. After two passages through a chilled French press cell at a pressure of 125 MPa, the soluble extract was separated from solid cell constituents by centrifugation at 72500 × *g* for 45 min. The supernatant was loaded onto a 2 mL *Strep*-Tactin Superflow column (IBA), which was previously equilibrated with resuspension buffer. After washing with at least 6 column volumes of resuspension buffer, the protein was eluted in resuspension buffer containing 5 mM desthiobiotin. A final concentration of 20–30 mg mL^{-1} of purified protein was achieved after concentration with Ultra Centrifugal Filter Units (Amicon).

In order to obtain *Ht*SH protein with homogenous subunit stoichiometry, size exclusion chromatography was conducted after affinity chromatography. An amount of 200 µL of the concentrated *Ht*SH eluate was loaded onto a Superdex 200 10/300 GL column which was previously equilibrated with the same buffer used for affinity chromatography. Using an ÄKTA pure system, the flow rate was held at 0.2 mL min^{-1}, and protein elution occurred at approximately 0.3 column volumes as observed by an UV/vis absorption increase at 280 nm and 420 nm. Protein fractions of 0.4 mL were collected, and the *Ht*SH subunit composition was checked by SDS-PAGE according to Laemmli et al. [74]. After determining the H_2-dependent reduction of NAD$^+$ activity, fractions with highest specific activities and homogeneity were pooled and again concentrated using Ultra Centrifugal Filter Units (molecular weight cut-off of 100 kDa).

4.1.1. Enzyme assays

All enzyme measurements were performed in the presence of defined gas mixtures unless stated otherwise. Prior to use in enzyme assays, the buffers were bubbled with the respective gases. Buffers with 100% gas-saturation (1 bar, 50 °C) contained 720 µM H_2, 940 µM O_2 or 483 µM N_2. Buffers containing gas mixtures were prepared by mixing individual buffers with 100% gas saturation. The head space of the reaction vessels was kept as small as possible to avoid degassing of solutions. H_2-driven NAD$^+$ reduction of purified *Ht*SH in soluble extracts was determined at 50 °C in a buffer-filled, rubber-stoppered cuvette. The reactions were started by the addition of enzyme, and the absorbance increase at 365 nm due to NADH accumulation was monitored spectrophotometrically with a Cary 50 (Varian). The pH-dependent *Ht*SH activity was measured by using two different strategies. First, to minimize the influence of different buffer components on SH activity, a broad-range buffer system (pH 4.5–9) composed of 16 mM citrate, 16 mM Tris, and 16 mM glycine was used. The buffer system was adjusted at 50 °C with appropriate acids or bases to the desired pH values. Second, SH activity was also tested in the individual buffers mentioned above. Temperature-dependent activity measurements were performed in 50 mM bis-Tris, pH 6.5, containing 0.75 mM TCEP (replacing DTT), 0.5 mM $NiCl_2$, 5 mM $MgCl_2$ and 2 µM FMN. This owes to the fact that DTT precipitates in $NiCl_2$- and $MgCl_2$-containing 50 mM KPO_i buffer at temperatures above 40 °C.

NADH-driven H_2 production was measured with a modified Clark-type electrode [75] at 50 °C in 50 mM bis-Tris, pH 6.5, containing 5 mM $MgCl_2$, 0.5 mM $NiCl_2$, 0.75 mM TCEP, 2 µM FMN and 1 mM NADH. The buffers as well as the additives were gassed with N_2 before mixing, and the reaction was started by the addition of enzyme. Diaphorase activity of the SH was recorded spectrophotometrically as NADH-dependent benzyl viologen reduction at 50 °C in buffers with different pH values (composition see above), containing 5 mM benzyl viologen (BV), 1 mM NADH, and 90 µM dithionite. H_2-dependent reduction of BV (5 mM) was tested at 50 °C in buffers with different pH values (composition see above). Prior to use, the buffers were saturated with H_2.

In order to determine affinity constants for NAD^+ or NADH, the initial reaction velocities for H_2-dependent NAD^+ and NADH-dependent BV reduction, respectively, were measured at 50 °C and varying substrate concentrations. The recorded slopes were plotted against the substrate concentration and fitted to the Michaelis-Menten kinetic using the program Origin 2016.

Determination of affinity towards H_2 was performed amperometrically by mixing different volumes of H_2- and N_2-saturated buffers (50 mM bis-Tris, pH 6.5, 5 mM $MgCl_2$, 0.5 mM $NiCl_2$) to a total volume of 1.3 mL in the reaction chamber of a modified Clark electrode. The assay contained further the natural electron acceptor, NAD^+ (1 mM), in addition to 0.75 mM TCEP, and 2 μM FMN. The reaction was started by enzyme addition, and the resulting current change was recorded. The derived reaction velocities were plotted against the H_2 concentration and fitted to the Hill equation using Origin 2016.

4.1.2. Protein, iron, and FMN determination

The protein concentration was determined with the BCA™ Protein Assay Reagent Kit (Pierce, USA) using bovine serum albumin as the standard. The flavin mononucleotide concentration in protein samples was analyzed fluorometrically as described previously [30,31] Iron and nickel contents of purified *Ht*SH samples were analyzed by inductively coupled plasma optical emission spectroscopy (ICP-OES) as previously described [76]. Final numbers were derived from two biological replicates, while each sample was measured three times (three technical replicates).

4.1.3. Sample preparation for IR and EPR spectroscopy

For the characterization of as-isolated *Ht*SH, protein fractions were concentrated to approx. 0.3 mM using Amicon Ultra 0.5 mL Centrifugal Filters (Merck KGaA) and measured without further treatment. Samples of reduced *Ht*SH were prepared using different procedures. Prior to all reductive treatments, buffers were purged with Ar for 30 min, and O_2 was removed from protein samples by ten consecutive cycles of Ar purging and vacuum exertion. Partial reduction of the enzyme was achieved by 30 min incubation of 0.03 mM *Ht*SH with 2 mM TCEP and 5 mM NADH at 50 °C in an anaerobic, N_2-filled glovebox. After these treatments, the samples were concentrated to approx. 0.3 mM, and IR transmission cells and EPR tubes were purged with N_2 prior to loading. To further reduce *Ht*SH, solutions containing 0.03 mM of protein were incubated with 2 mM TCEP, 5 mM NADH, and 1 bar O_2-free H_2 (O_2 was removed using a Varian Gas Clean Oxygen Filter PIN CP17970) in H_2-saturated buffer at 50 °C for 30 min in an anaerobic chamber (95% N_2, 5% H_2). The H_2 stream was enriched with H_2O to avoid sample drying. Prior to measurements, samples were concentrated to ~0.3 mM, and IR transmission cells and EPR tubes were purged with H_2. Aliquots of all samples were directly injected into an IR transmission cell for subsequent characterization, while the remainder was transferred to EPR tubes, quenched in cold ethanol (ca. 210 K) and stored in liquid nitrogen for further analysis.

4.1.4. IR spectroscopy

IR spectra of 0.3 mM solutions of as-isolated and chemically reduced *Ht*SH were recorded with a spectral resolution of 2 cm^{-1} using a Bruker Tensor 27 FTIR spectrometer, equipped with a liquid nitrogen-cooled MCT detector. The sample compartment was purged with dry air, and the sample was held in a temperature-controlled (10 °C) gas-tight IR transmission cell for liquid samples (volume: 10 μL, optical path length: 50 μm), equipped with CaF_2 windows. The Bruker OPUS software, version 5.5 or higher, was used for data acquisition and evaluation.

4.1.5. IR spectro-electrochemical experiments

IR spectro-electrochemical experiments were performed on ca. 0.3 mM solutions of *Ht*SH, activated anaerobically with 2 mM TCEP, using an Optically Transparent Thin Layer Electrochemical (OTTLE) cell [77] with an optical path length below 10 μm. In order to avoid protein adsorption, the gold mesh working electrode was incubated anaerobically with a mixed self-assembling monolayer of 1 mM cysteamine and 1 mM mercaptopropionic acid, solved in ethanol, for 30 min. Preparation of the OTTLE cell was performed anaerobically in an Ar-filled box. The following redox mediators were added to the protein solution in order to ensure fast equilibration at the applied potentials (0.5 mM each, potential vs. SHE): TMPPO (+ 262 mV), 1,2-naphthoquinone (+ 145 mV), 1,4-naphthoquinone (+ 60 mV), methylene blue (+ 11 mV), indigo trisulfate (− 80 mV), indigo disulfate (− 130 mV), 2-hydroxy-1,2-naphthoquinone (− 139 mV), resorufin (− 195 mV), anthraquinone-2-sulfonate (− 225 mV), safranin T (− 290 mV), benzyl viologen (− 358 mV), methyl viologen (− 446 mV) [77–79]. Potential-dependent IR spectra with a resolution of 2 cm^{-1} were recorded at 30 °C using a Bruker IFS 66 v/s FTIR spectrometer equipped with a liquid nitrogen-cooled MCT detector. The Bruker OPUS software, version 5.5 or higher, was used for data acquisition and evaluation. Potential control was accomplished using a Model 263A Potentiostat (Princeton Applied Science) and the PARControl 1.05 software. Samples were equilibrated at all potentials for at least 3 min until the corresponding IR spectrum remained unchanged.

4.1.6. EPR spectroscopy

A Bruker EMXplus spectrometer equipped with an ER 4122 SHQE resonators and an Oxford EPR 900 helium flow cryostat with temperature control (Oxford ITC4) between 5 and 310 K was used in the experiments. Spectra were baseline-corrected by subtracting a background spectrum obtained from buffer solution using the same experimental parameters. Experimental conditions: 1 mW microwave power, microwave frequency: 9.29 GHz, 1 mT modulation amplitude, 100 kHz modulation frequency. Spectra simulations were performed using the MATLAB toolbox EasySpin (version 5.1.7).

4.1.7. NRVS spectroscopy

For nuclear resonance vibrational spectroscopy (NRVS), *R. eutropha* HF1054 (pJP09) was cultured as described above, with the exception that 18 μM $^{57}FeCl_2$ instead of $^{56}FeCl_2$ was used as the iron source. The resulting ^{57}Fe-labelled *Ht*SH was purified via *Strep*-Tactin affinity chromatography. NRVS was performed at SPring-8 BL09XU with a 0.8 meV (6.5 cm^{-1}) energy resolution at 14.4125 keV as described previously [43]. The beam size at BL09XU was 1.1 mm (horizontal) × 0.6 mm (vertical). A 4-element avalanche photo diode detector array was used to measure delayed K shell fluorescence and nuclear fluorescence by ^{57}Fe atoms. All measurements were performed in the cryostat base that was cooled to 10 K. The real sample temperature was 30–60 K, as obtained from the spectral analysis. The raw NRVS data was converted to a ^{57}Fe partial vibrational density of states (PVDOS) by the PHOENIX software [80], while the energy scale was calibrated with an external reference ($[NEt_4][FeCl_4]$). For the *Ht*SH protein sample (22 μL, 0.8 mM), the accumulation time was 21 h.

Transparency document

The Transparency document associated with this article can be found, in online version.

Acknowledgements

We are grateful to Thomas Lonsdale (University of Oxford) for initial biochemical analyses of purified *Ht*SH. We thank the group of Professor Silke Leimkühler (Universität Postdam) for metal determination. J.P. and S.W. are grateful for receiving scholarships from the Berlin International Graduate School for Natural Science & Engineering (BIG-NSE). This work was supported by the Deutsche Forschungsgemeinschaft (DFG) through the Cluster of Excellence, Unifying Concepts in Catalysis (UniCat, EXC 314), and the priority

program “Iron-Sulfur for Life” (SPP 1927). The NRVS experiments were performed at BL09XU of SPring8 approved under JASRI proposal number2014B1032. S. P. Cramer is indebted to the Einstein Foundation (Berlin) for support through an Einstein Visiting Fellowship.

Appendix A. Supplementary data

Supplementary data to this article can be found online at https://doi.org/10.1016/j.bbabio.2017.09.006.

References

[1] P.M. Vignais, B. Billoud, Occurrence, classification, and biological function of hydrogenases: an overview, Chem. Rev. 107 (2007) 4206–4272.
[2] E. Schwartz, J. Fritsch, B. Friedrich, H_2-Metabolizing prokaryotes, in: E. Rosenberg, E.F. DeLong, S. Lory, E. Stackebrandt, F. Thompson (Eds.), The Prokaryotes, Springer Berlin Heidelberg, Berlin, Heidelberg, 2013, pp. 119–199.
[3] W. Lubitz, H. Ogata, O. Rüdiger, E. Reijerse, Hydrogenases, Chem. Rev. 114 (2014) 4081–4148.
[4] J. Fritsch, O. Lenz, B. Friedrich, Structure, function and biosynthesis of O_2-tolerant hydrogenases, Nat. Rev. Microbiol. 11 (2013) 106–114.
[5] O. Lenz, L. Lauterbach, S. Frielingsdorf, B. Friedrich, Oxygen-tolerant hydrogenases and their biotechnological potential, in: M. Rögner (Ed.), Biohydrogen, De Gruyter, 2015, pp. 61–88.
[6] M. Horch, L. Lauterbach, O. Lenz, P. Hildebrandt, I. Zebger, NAD(H)-coupled hydrogen cycling - structure-function relationships of bidirectional [NiFe] hydrogenases, FEBS Lett. 586 (2012) 545–556.
[7] E. van der Linden, B.W. Faber, B. Bleijlevens, T. Burgdorf, M. Bernhard, B. Friedrich, S.P. Albracht, Selective release and function of one of the two FMN groups in the cytoplasmic NAD^+-reducing [NiFe]-hydrogenase from *Ralstonia eutropha*, Eur. J. Biochem. 271 (2004) 801–808.
[8] E. van der Linden, T. Burgdorf, A.L. de Lacey, T. Buhrke, M. Scholte, V.M. Fernandez, B. Friedrich, S.P. Albracht, An improved purification procedure for the soluble [NiFe]-hydrogenase of *Ralstonia eutropha*: new insights into its (in)stability and spectroscopic properties, J. Biol. Inorg. Chem. 11 (2006) 247–260.
[9] R.G. Efremov, L.A. Sazanov, The coupling mechanism of respiratory complex I - a structural and evolutionary perspective, Biochim. Biophys. Acta 1817 (2012) 1785–1795.
[10] T. Friedrich, D. Scheide, The respiratory complex I of bacteria, archaea and eukarya and its module common with membrane-bound multisubunit hydrogenases, FEBS Lett. 479 (2000) 1–5.
[11] R. Baradaran, J.M. Berrisford, G.S. Minhas, L.A. Sazanov, Crystal structure of the entire respiratory complex I, Nature 494 (2013) 443–448.
[12] M. Horch, L. Lauterbach, M. Saggu, P. Hildebrandt, F. Lendzian, R. Bittl, O. Lenz, I. Zebger, Probing the active site of an O_2-tolerant NAD^+-reducing [NiFe]-hydrogenase from *Ralstonia eutropha* H16 by in situ EPR and FTIR spectroscopy, Angew. Chem. Int. Ed. Eng. 49 (2010) 8026–8029.
[13] K. Karstens, S. Wahlefeld, M. Horch, M. Grunzel, L. Lauterbach, F. Lendzian, I. Zebger, O. Lenz, Impact of the iron-sulfur cluster proximal to the active site on the catalytic function of an O_2-tolerant NAD^+-reducing [NiFe]-hydrogenase, Biochemistry 54 (2015) 389–403.
[14] K. Schneider, H.G. Schlegel, Production of superoxide radicals by soluble hydrogenase from *Alcaligenes eutrophus* H16, Biochem. J. 193 (1981) 99–107.
[15] L. Lauterbach, O. Lenz, Catalytic production of hydrogen peroxide and water by oxygen-tolerant [NiFe]-hydrogenase during H_2 cycling in the presence of O_2, J. Am. Chem. Soc. 135 (2013) 17897–17905.
[16] T.H. Lonsdale, L. Lauterbach, S. Honda Malca, B.M. Nestl, B. Hauer, O. Lenz, H_2-driven biotransformation of *n*-octane to 1-octanol by a recombinant *Pseudomonas putida* strain co-synthesizing an O_2-tolerant hydrogenase and a P450 monooxygenase, Chem. Commun. 51 (2015) 16173–16175.
[17] A.K. Holzer, K. Hiebler, F.G. Mutti, R.C. Simon, L. Lauterbach, O. Lenz, W. Kroutil, Asymmetric biocatalytic amination of ketones at the expense of NH_3 and molecular hydrogen, Org. Lett. 17 (2015) 2431–2433.
[18] H.A. Reeve, L. Lauterbach, P.A. Ash, O. Lenz, K.A. Vincent, A modular system for regeneration of NAD cofactors using graphite particles modified with hydrogenase and diaphorase moieties, Chem. Commun. (Camb.) 48 (2011) 1589–1591.
[19] H.A. Reeve, L. Lauterbach, O. Lenz, K.A. Vincent, Enzyme-modified particles for selective biocatalytic hydrogenation by hydrogen-driven NADH recycling, ChemCatChem 7 (2015) 3480–3487.
[20] J. Ratzka, L. Lauterbach, O. Lenz, M.B. Ansorge-Schumacher, Systematic evaluation of the dihydrogen-oxidising and NAD^+-reducing soluble [NiFe]-hydrogenase from *Ralstonia eutropha* H16 as a cofactor regeneration catalyst, Biocatal. Biotransformation 29 (2011) 246–252.
[21] N.R. Hayashi, T. Ishida, A. Yokota, T. Kodama, Y. Igarashi, *Hydrogenophilus thermoluteolus* gen. nov., sp. nov., a thermophilic, facultatively chemolithoautotrophic, hydrogen-oxidizing bacterium, Int. J. Syst. Bacteriol. 49 (1999) 783–786.
[22] E. Goto, T. Kodama, Y. Minoda, Growth and taxonomy of thermophilic hydrogen bacteria, Agric. Biol. Chem. 42 (2014) 1305–1308.
[23] M. Taketa, H. Nakagawa, M. Habukawa, H. Osuka, K. Kihira, H. Komori, N. Shibata, M. Ishii, Y. Igarashi, H. Nishihara, K.-S. Yoon, S. Ogo, Y. Shomura, Y. Higuchi, Crystallization and preliminary X-ray analysis of the NAD^+-reducing NiFe hydrogenase from *Hydrogenophilus thermoluteolus* TH-1, Acta Crystallogr. F Struct. Biol. Commun. 71 (2015) 96–99.
[24] T. Burgdorf, E. van der Linden, M. Bernhard, Q.Y. Yin, J.W. Back, A.F. Hartog, A.O. Muijsers, C.G. de Koster, S.P.J. Albracht, B. Friedrich, The soluble NAD^+-reducing NiFe-hydrogenase from *Ralstonia eutropha* H16 consists of six subunits and can be specifically activated by NADPH, J. Bacteriol. 187 (2005) 3122–3132.
[25] T. Goris, A.F. Wait, M. Saggu, J. Fritsch, N. Heidary, M. Stein, I. Zebger, F. Lendzian, F.A. Armstrong, B. Friedrich, O. Lenz, A unique iron-sulfur cluster is crucial for oxygen tolerance of a [NiFe]-hydrogenase, Nat. Chem. Biol. 7 (2011) 310–318.
[26] J. Dernedde, T. Eitinger, N. Patenge, B. Friedrich, *hyp* gene products in *Alcaligenes eutrophus* are part of a hydrogenase-maturation system, Eur. J. Biochem. 235 (1996) 351–358.
[27] I. Wolf, T. Buhrke, J. Dernedde, A. Pohlmann, B. Friedrich, Duplication of *hyp* genes involved in maturation of [NiFe] hydrogenases in *Alcaligenes eutrophus* H16, Arch. Microbiol. 170 (1998) 451–459.
[28] I. Bürstel, E. Siebert, S. Frielingsdorf, I. Zebger, B. Friedrich, O. Lenz, CO synthesized from the central one-carbon pool as source for the iron carbonyl in O_2-tolerant NiFe-hydrogenase, Proc. Natl. Acad. Sci. U. S. A. 113 (2016) 14722–14726.
[29] K. Schneider, H.G. Schlegel, K. Jochim, Effect of nickel on activity and subunit composition of purified hydrogenase from *Nocardia opaca* 1 b, Eur. J. Biochem. 138 (1984) 533–541.
[30] K. Schneider, H.G. Schlegel, Purification and properties of soluble hydrogenase from *Alcaligenes eutrophus* H 16, Biochim. Biophys. Acta 452 (1976) 66–80.
[31] L. Lauterbach, Z. Idris, K.A. Vincent, O. Lenz, Catalytic properties of the isolated diaphorase fragment of the NAD-reducing [NiFe]-hydrogenase from *Ralstonia eutropha*, PLoS One 6 (2011) e25939.
[32] O. Schmitz, G. Boison, H. Salzmann, H. Bothe, K. Schutz, S.-h. Wang, T. Happe, HoxE - a subunit specific for the pentameric bidirectional hydrogenase complex (HoxEFUYH) of cyanobacteria, Biochim. Biophys. Acta 1554 (2002) 66–74.
[33] K. Ma, R. Weiss, M.W.W. Adams, Characterization of hydrogenase II from the hyperthermophilic archaeon *Pyrococcus furiosus* and assessment of its role in sulfur reduction, J. Bacteriol. 182 (2000) 1864–1871.
[34] L.T. Serebryakova, M. Medina, N.A. Zorin, I.N. Gogotov, R. Cammack, Reversible hydrogenase of *Anabaena variabilis* ATCC 29413: catalytic properties and characterization of redox centres, FEBS Lett. 383 (1996) 79–82.
[35] L. Cournac, G. Guedeney, G. Peltier, P.M. Vignais, Sustained photoevolution of molecular hydrogen in a mutant of *Synechocystis* sp. strain PCC 6803 deficient in the type I NADPH-dehydrogenase complex, J. Bacteriol. 186 (2004) 1737–1746.
[36] K. Gutekunst, X. Chen, K. Schreiber, U. Kaspar, S. Makam, J. Appel, The bidirectional NiFe-hydrogenase in *Synechocystis* sp. PCC 6803 is reduced by flavodoxin and ferredoxin and is essential under mixotrophic, nitrate-limiting conditions, J. Biol. Chem. 289 (2014) 1930–1937.
[37] S.K. Chandrayan, P.M. McTernan, R.C. Hopkins, J. Sun, F.E. Jenney, M.W.W. Adams, Engineering hyperthermophilic archaeon *Pyrococcus furiosus* to overproduce its cytoplasmic NiFe-hydrogenase, J. Biol. Chem. 287 (2012) 3257–3264.
[38] K. Ma, R.N. Schicho, R.M. Kelly, M.W. Adams, Hydrogenase of the hyperthermophile *Pyrococcus furiosus* is an elemental sulfur reductase or sulfhydrogenase: evidence for a sulfur-reducing hydrogenase ancestor, Proc. Natl. Acad. Sci. U. S. A. 90 (1993) 5341–5344.
[39] F.O. Bryant, M.W. Adams, Characterization of hydrogenase from the hyperthermophilic archaebacterium, *Pyrococcus furiosus*, J. Biol. Chem. 264 (1989) 5070–5079.
[40] F. Germer, I. Zebger, M. Saggu, F. Lendzian, R. Schulz, J. Appel, Overexpression, isolation, and spectroscopic characterization of the bidirectional NiFe hydrogenase from *Synechocystis* sp. PCC 6803, J. Biol. Chem. 284 (2009) 36462–36472.
[41] P. Kwan, C.L. McIntosh, D.P. Jennings, R.C. Hopkins, S.K. Chandrayan, C.-H. Wu, M.W.W. Adams, A.K. Jones, The NiFe-hydrogenase of *Pyrococcus furiosus* exhibits a new type of oxygen tolerance, J. Am. Chem. Soc. 137 (2015) 13556–13565.
[42] H. Ogata, T. Kramer, H. Wang, D. Schilter, V. Pelmenschikov, M. van Gastel, F. Neese, T.B. Rauchfuss, L.B. Gee, A.D. Scott, Y. Yoda, Y. Tanaka, W. Lubitz, S.P. Cramer, Hydride bridge in NiFe-hydrogenase observed by nuclear resonance vibrational spectroscopy, Nat. Commun. 6 (2015) 7890.
[43] L. Lauterbach, H. Wang, M. Horch, L.B. Gee, Y. Yoda, Y. Tanaka, I. Zebger, O. Lenz, S.P. Cramer, Nuclear resonance vibrational spectroscopy reveals the FeS cluster composition and active site vibrational properties of an O_2-tolerant NAD^+-reducing [NiFe] hydrogenase, Chem. Sci. 6 (2015) 1055–1060.
[44] Y. Xiao, M.-L. Tan, T. Ichiye, H. Wang, Y. Guo, M.C. Smith, J. Meyer, W. Sturhahn, E.E. Alp, J. Zhao, Y. Yoda, S.P. Cramer, Dynamics of *Rhodobacter capsulatus* 2Fe-2S ferredoxin VI and *Aquifex aeolicus* ferredoxin 5 via nuclear resonance vibrational spectroscopy (NRVS) and resonance Raman spectroscopy, Biochemistry 47 (2008) 6612–6627.
[45] D. Mitra, V. Pelmenschikov, Y. Guo, D.A. Case, H. Wang, W. Dong, M.-L. Tan, T. Ichiye, F.E. Jenney, M.W.W. Adams, Y. Yoda, J. Zhao, S.P. Cramer, Dynamics of the 4Fe-4S cluster in *Pyrococcus furiosus* D14C ferredoxin via nuclear resonance vibrational and resonance Raman spectroscopies, force field simulations, and density functional theory calculations, Biochemistry 50 (2011) 5220–5235.
[46] A. Volbeda, E. Garcin, C. Piras, A.L. DeLacey, V.M. Fernandez, E.C. Hatchikian, M. Frey, J.C. FontecillaCamps, Structure of the [NiFe] hydrogenase active site: evidence for biologically uncommon Fe ligands, J. Am. Chem. Soc. 118 (1996) 12989–12996.
[47] R.P. Happe, W. Roseboom, A.J. Pierik, S.P. Albracht, K.A. Bagley, Biological activation of hydrogen, Nature 385 (1997) 126.
[48] K.A. Bagley, E.C. Duin, W. Roseboom, S.P.J. Albracht, W.H. Woodruff, Infrared-detectable group senses changes in charge density on the nickel center in hydrogenase from *Chromatium vinosum*, Biochemistry 34 (1995) 5527–5535.
[49] M.Y. Darensbourg, E.J. Lyon, J.J. Smee, The bio-organometallic chemistry of active

site iron in hydrogenases, Coord. Chem. Rev. 206–207 (2000) 533–561.
[50] M. Horch, L. Lauterbach, M.A. Mroginski, P. Hildebrandt, O. Lenz, I. Zebger, Reversible active site sulfoxygenation can explain the oxygen tolerance of a NAD^+-reducing [NiFe] hydrogenase and its unusual infrared spectroscopic properties, J. Am. Chem. Soc. 137 (2015) 2555–2564.
[51] B.L. Greene, C.-H. Wu, P.M. McTernan, M.W.W. Adams, R.B. Dyer, Proton-coupled electron transfer dynamics in the catalytic mechanism of a NiFe-hydrogenase, J. Am. Chem. Soc. 137 (2015) 4558–4566.
[52] L. Lauterbach, J. Liu, M. Horch, P. Hummel, A. Schwarze, M. Haumann, K.A. Vincent, O. Lenz, I. Zebger, The hydrogenase subcomplex of the NAD^+-reducing [NiFe] hydrogenase from *Ralstonia eutropha* - Insights into catalysis and redox interconversions, Eur. J. Inorg. Chem. 2011 (2011) 1067–1079.
[53] R.P. Happe, W. Roseboom, G. Egert, C.G. Friedrich, C. Massanz, B. Friedrich, S.P.J. Albracht, Unusual FTIR and EPR properties of the H_2-activating site of the cytoplasmic NAD-reducing hydrogenase from *Ralstonia eutropha*, FEBS Lett. 466 (2000) 259–263.
[54] E. van der Linden, T. Burgdorf, M. Bernhard, B. Bleijlevens, B. Friedrich, S.P. Albracht, The soluble [NiFe]-hydrogenase from *Ralstonia eutropha* contains four cyanides in its active site, one of which is responsible for the insensitivity towards oxygen, J. Biol. Inorg. Chem. 9 (2004) 616–626.
[55] S.T. Stripp, B. Soboh, U. Lindenstrauss, M. Braussemann, M. Herzberg, D.H. Nies, R.G. Sawers, J. Heberle, HypD is the scaffold protein for Fe-$(CN)_2$CO cofactor assembly in [NiFe]-hydrogenase maturation, Biochemistry 52 (2013) 3289–3296.
[56] M. Horch, P. Hildebrandt, I. Zebger, Concepts in bio-molecular spectroscopy: vibrational case studies on metalloenzymes, Phys. Chem. Chem. Phys. 17 (2015) 18222–18237.
[57] K. Schneider, R. Cammack, H.G. Schlegel, D.O. Hall, The iron-sulphur centres of soluble hydrogenase from *Alcaligenes eutrophus*, Biochim. Biophys. Acta 578 (1979) 445–461.
[58] K. Schneider, R. Cammack, H.G. Schlegel, Content and localization of FMN, Fe-S clusters and nickel in the NAD-linked hydrogenase of *Nocardia opaca* 1b, Eur. J. Biochem. 142 (1984) 75–84.
[59] C. Zaborosch, M. Köstert, E. Bill, K. Schneider, H. Schlegel, A. Trautweint, EPR and Mössbauer spectroscopic studies on the tetrameric, NAD-linked hydrogenase of *Nocardia opaca* 1b and its two dimers: 1. The βδ-dimer - a prototype of a simple hydrogenase, Biometals 8 (1995).
[60] A. Erkens, K. Schneider, A. Müller, The NAD-linked soluble hydrogenase from *Alcaligenes eutrophus* H16: detection and characterization of EPR signals deriving from nickel and flavin, J. Biol. Inorg. Chem. 1 (1996) 99–110.
[61] P.J. Silva, B. de Castro, W.R. Hagen, On the prosthetic groups of the NiFe sulfhydrogenase from *Pyrococcus furiosus*: topology, structure, and temperature-dependent redox chemistry, J. Biol. Inorg. Chem. 4 (1999) 284–291.
[62] J. Löwenstein, L. Lauterbach, C. Teutloff, O. Lenz, R. Bittl, Active site of the NAD^+-reducing hydrogenase from *Ralstonia eutropha* studied by EPR spectroscopy, J. Phys. Chem. B 119 (2015) 13834–13841.
[63] R. Cammack, D.S. Patil, E. Hatchikian, V.M. Fernández, Nickel and iron-sulphur centres in *Desulfovibrio gigas* hydrogenase: ESR spectra, redox properties and interactions, Biochim. Biophys. Acta 912 (1987) 98–109.
[64] B. Guigliarelli, C. More, A. Fournel, M. Asso, E.C. Hatchikian, R. Williams, R. Cammack, P. Bertrand, Structural organization of the Ni and (4Fe-4S) centers in the active form of *Desulfovibrio gigas* hydrogenase. Analysis of the magnetic interactions by electron paramagnetic resonance spectroscopy, Biochemistry 34 (1995) 4781–4790.
[65] R.M. Kelly, J.W. Deming, Extremely thermophilic archaebacteria: biological and engineering considerations, Biotechnol. Prog. 4 (1988) 47–62.
[66] T. Reda, C.D. Barker, J. Hirst, Reduction of the iron-sulfur clusters in mitochondrial NADH:ubiquinone oxidoreductase (complex I) by EuII-DTPA, a very low potential reductant, Biochemistry 47 (2008) 8885–8893.
[67] T. Ohnishi, Iron–sulfur clusters/semiquinones in complex I, Biochim. Biophys. Acta 1364 (1998) 186–206.
[68] E. Nakamaru-Ogiso, T. Yano, T. Yagi, T. Ohnishi, Characterization of the iron-sulfur cluster N7 (N1c) in the subunit NuoG of the proton-translocating NADH-quinone oxidoreductase from *Escherichia coli*, J. Biol. Chem. 280 (2005) 301–307.
[69] A. Porthun, M. Bernhard, B. Friedrich, Expression of a functional NAD-reducing [NiFe] hydrogenase from the gram-positive *Rhodococcus opacus* in the gram-negative *Ralstonia eutropha*, Arch. Microbiol. 177 (2002) 159–166.
[70] C.J. Marx, M.E. Lidstrom, Development of improved versatile broad-host-range vectors for use in methylotrophs and other Gram-negative bacteria, Microbiology 147 (2001) 2065–2075.
[71] E. Schwartz, U. Gerischer, B. Friedrich, Transcriptional regulation of *Alcaligenes eutrophus* hydrogenase genes, J. Bacteriol. 180 (1998) 3197–3204.
[72] L. Kleihues, O. Lenz, M. Bernhard, T. Buhrke, B. Friedrich, The H_2 sensor of *Ralstonia eutropha* is a member of the subclass of regulatory [NiFe] hydrogenases, J. Bacteriol. 182 (2000) 2716–2724.
[73] C. Massanz, S. Schmidt, B. Friedrich, Subforms and in vitro reconstitution of the NAD-reducing hydrogenase of *Alcaligenes eutrophus*, J. Bacteriol. 180 (1998) 1023–1029.
[74] U.K. Laemmli, Cleavage of structural proteins during the assembly of the head of bacteriophage T4, Nature 227 (1970) 680–685.
[75] R. Wang, F.P. Healey, J. Myers, Amperometric measurement of hydrogen evolution in *Chlamydomonas*, Plant Physiol. 48 (1971) 108–110.
[76] M. Neumann, G. Mittelstadt, F. Seduk, C. Iobbi-Nivol, S. Leimkuhler, MocA is a specific cytidylyltransferase involved in molybdopterin cytosine dinucleotide biosynthesis in *Escherichia coli*, J. Biol. Chem. 284 (2009) 21891–21898.
[77] D. Moss, E. Nabedryk, J. Breton, W. Mäntele, Redox-linked conformational changes in proteins detected by a combination of infrared spectroscopy and protein electrochemistry. Evaluation of the technique with cytochrome *c*, Eur. J. Biochem. 187 (1990) 565–572.
[78] A.L. de Lacey, E.C. Hatchikian, A. Volbeda, M. Frey, J.C. Fontecilla-Camps, V.M. Fernandez, Infrared-spectroelectrochemical characterization of the [NiFe] hydrogenase of *Desulfovibrio gigas*, J. Am. Chem. Soc. 119 (1997) 7181–7189.
[79] C. Fichtner, C. Laurich, E. Bothe, W. Lubitz, Spectroelectrochemical characterization of the NiFe hydrogenase of *Desulfovibrio vulgaris* Miyazaki F, Biochemistry 45 (2006) 9706–9716.
[80] W. Sturhahn, CONUSS and PHOENIX: evaluation of nuclear resonant scattering data, Hyperfine Interact. 125 (2000) 149–172.